


Cite this: *RSC Adv.*, 2017, 7, 18830

# Modulating Cu<sup>+</sup> distribution on the surface of Ce-doped CuO composite oxides for SO<sub>2</sub>-resistant NH<sub>3</sub>-selective catalytic reduction of NO

Mengmeng Xing, Qian Sun, Chun Zeng, Huize Wang, Dan Zhao, \* Ning Zhang and Sanguo Hong

A series of (CeO<sub>x</sub>)<sub>m</sub>CuO composite oxides with different Ce/Cu molar ratios (*m*) were prepared by co-precipitation for ammonia-selective catalytic reduction of NO (NH<sub>3</sub>-SCR-NO) in the absence and presence of SO<sub>2</sub>. Through X-ray diffraction (XRD), X-ray photoelectron spectroscopy (XPS), H<sub>2</sub>-temperature programmed reduction (H<sub>2</sub>-TPR), and NH<sub>3</sub>-temperature programmed desorption (NH<sub>3</sub>-TPD) characterization, it was demonstrated that the prepared samples were featured by distinguished Cu<sup>+</sup> distributions on the surface of the Ce-doped CuO composite structure, indicating a special interaction or synergistic effect present in the samples. The modulated distributions of Cu<sup>+</sup> achieved by adjusting the Ce/Cu molar ratio were found to be crucial for optimizing the redox ability and acid feature among the samples. The outstanding SO<sub>2</sub>-resistant NH<sub>3</sub>-SCR-NO performance (NO conversion close to 100% in temperature window of 250–350 °C under 200 ppm SO<sub>2</sub>-presence) was observed on (CeO<sub>x</sub>)<sub>0.25</sub>CuO which possessing the highest Cu<sup>+</sup> distribution, indicating the significant dependence of Cu<sup>+</sup> distribution in Cu-based catalysts on enhancing catalytic performance for NH<sub>3</sub>-SCR-NO. These results also suggested that the distinguished synergistic effect among binary component Cu-based catalysts should be considered as an important factor to govern the performance of NH<sub>3</sub>-SCR-NO<sub>x</sub>, which could be inferred as important clues to innovate more efficient catalysts for NH<sub>3</sub>-SCR-NO<sub>x</sub>, as well as other heterogeneous catalysis applications based on Cu-catalysts.

Received 14th January 2017

Accepted 14th March 2017

DOI: 10.1039/c7ra00581d

rsc.li/rsc-advances

## 1. Introduction

Nitric oxides (NO<sub>x</sub>) are a type of major gaseous pollutant that cause many harmful effects on both the environment and human health and are inevitably produced from fossil fuel combustion processes of power plants and vehicles.<sup>1</sup> For abatement of their emissions to the atmosphere, in view of current technique, the most efficient way is converting them to harmless N<sub>2</sub> and H<sub>2</sub>O at the beginning of emissions by NH<sub>3</sub> through selective catalytic reduction (NH<sub>3</sub>-SCR-NO<sub>x</sub>) process over heterogeneous catalysts.<sup>2,3</sup> V<sub>2</sub>O<sub>5</sub>-WO<sub>3</sub>-TiO<sub>2</sub> has been used as a commercial catalyst for NH<sub>3</sub>-SCR-NO<sub>x</sub>, but it has drawbacks such as a narrow working temperature window, use of toxic vanadium species, and low N<sub>2</sub> selectivity at high temperatures,<sup>4–6</sup> which motivated a new wave of innovation towards more efficient and environmentally friendly replacement catalysts for NH<sub>3</sub>-SCR-NO<sub>x</sub>. Among various attempts, copper-based catalysts supported on oxides or zeolites have recently emerged as attractive candidates due to their environmentally benign characteristics and high SCR performance in a wide temperature range.<sup>7–10</sup> Co, Fe, Mn, and Ce have been doped into

the phase or co-deposited with Cu on supports, such as zeolites, TiO<sub>2</sub>, and SiO<sub>2</sub>, to fabricate composite Cu-based NH<sub>3</sub>-SCR catalysts. Addition of these elements was found to be beneficial for creating charge imbalance, vacancies or unsaturated chemical bonds on the catalysts surface, and practical contribution to the catalytic improvements for NH<sub>3</sub>-SCR-NO<sub>x</sub>.<sup>11–15</sup> These positive influences originated *via* an additive introducing method were profoundly defined as synergistic effect among different components. However, essential knowledge of this effect among current Cu-based NH<sub>3</sub>-SCR-NO<sub>x</sub> catalysts is still controversial.

In general, the so-called synergistic effect was always discussed as an interaction between the two components of the composite samples. Since most of the present Cu-based NH<sub>3</sub>-SCR-NO<sub>x</sub> catalysts can be roughly sorted as ternary-component composites composed of Cu species, assistant additives, and a supporter, there were at least three different interactions, Cu-supporter, Cu-additive, and additive-support, those could be involved in the composite structures, which led to inconsistent views on the origin and function of the synergistic effect. A popular view was mainly focused on the Cu-additive interaction, and additive-induced geometric modifications or electronic interactions were believed to be responsible for the observed enhancement in the catalytic performance. For instance, Dou

Institute of Applied Chemistry, College of Chemistry, Nanchang University, Nanchang, Jiangxi 330031, China. E-mail: zhaodan@ncu.edu.cn; Tel: +86-15879176996



*et al.*<sup>7</sup> demonstrated that Ce doping improved the redox properties of Cu–Ce/ZSM-5 catalyst by enhancing the composition of Cu species in high valence and mobility of lattice oxygen compared to those of the Cu/ZSM-5 catalyst. Similar descriptions were also found on supported Cu–Fe or Cu–Mn catalysts.<sup>11,16,17</sup> However, the interactions between active component and supporter were always ignored in these studies, and the situation was quite doubtful for current Cu-based NH<sub>3</sub>-SCR-NO<sub>x</sub> catalysts since this interaction was usually present as a significant factor to resolve the catalytic behaviors of supported metal or metal oxides catalysts.<sup>18–20</sup> This is especially true in view of the low loadings of both Cu species and additives on supporters. In contrast, it is not a surprise that some more complicated synergistic effects such as the dual redox cycles among Cu–Ce–Ti triplet complex on Cu–Ce/TiO<sub>2</sub> catalysts were supposed to be the key factor for enhancing the performance of NH<sub>3</sub>-SCR-NO.<sup>21</sup> To clarify these arguments, a basic work could be decreasing the complexity of the catalysts such as *via* employing binary component samples as catalysts. To the best of our knowledge, these works, especially in directly constructing and systematically modulating the composite structure of binary component Cu-based NH<sub>3</sub>-SCR-NO<sub>x</sub> catalysts, have been seldom reported.<sup>22</sup> In addition, one of the main drawbacks of current Cu-based NH<sub>3</sub>-SCR-NO<sub>x</sub> catalysts is their poor resistance to SO<sub>2</sub>,<sup>23,24</sup> and to date, research has been focused on simple composition catalysts, whereas binary component samples for SO<sub>2</sub>-resistant NH<sub>3</sub>-SCR-NO<sub>x</sub> are still scarce.

In this study, a series of Cu–Ce composite oxides with systematic change in Cu/Ce molar ratio was prepared by a common co-precipitation method and was aimed at NH<sub>3</sub>-SCR of NO in the absence and presence of SO<sub>2</sub>. Compared to the absolute existence of Cu<sup>2+</sup> on Cu–Ce-supporter ternary-component samples reported in literatures, the distinguished Cu<sup>+</sup> distributions in the surface of Ce-doped CuO composite structure suggested that a kind of special interaction or synergistic effect existed on our samples. By properly modulating the distribution of Cu<sup>+</sup> in these Cu–Ce binary composite oxides with a controlled Cu/Ce molar ratio and thermal processing temperature, superior SO<sub>2</sub>-resistant activity for NH<sub>3</sub>-SCR of NO was achieved. These results suggested that the distinguished synergistic effect among binary component Cu-based catalysts compared to popular ternary-component samples should be noticed as a type of significant factor to govern the performance for NH<sub>3</sub>-SCR-NO<sub>x</sub>, which could be inferred as important clues to innovate more efficient catalysts for NH<sub>3</sub>-SCR-NO<sub>x</sub>, as well as other heterogeneous catalysis applications upon Cu catalysts.

## 2. Experimental

### 2.1. Preparation of samples

Cu–Ce composite oxides with different Cu/Ce molar ratios were prepared *via* the co-precipitation of Cu(CH<sub>3</sub>COO)<sub>2</sub> and Ce(NO<sub>3</sub>)<sub>3</sub> with Na<sub>2</sub>CO<sub>3</sub> as a precipitant. Simply, desired amounts of Cu(CH<sub>3</sub>COO)<sub>2</sub>·H<sub>2</sub>O and Ce(NO<sub>3</sub>)<sub>3</sub>·6H<sub>2</sub>O were dissolved in deionized water and then 0.1 M Na<sub>2</sub>CO<sub>3</sub> aqueous

solution was added to the abovementioned mixture under vigorous stirring to adjust the pH of the system to 9. The solution was stirred at room temperature for 1 h and subsequently the solid powders were filtered out and washed with deionized water several times. After being dried at 110 °C in air for 5 h, the powders were calcined in a muffle furnace at 350 °C for 3 h to obtain catalyst samples. The compositions of all the samples were measured by the ICP-OES technique, and according to the measurements and the calcination temperature, the three Cu–Ce composite oxides obtained were labelled as (CeO<sub>x</sub>)<sub>0.125</sub>CuO-350, (CeO<sub>x</sub>)<sub>0.25</sub>CuO-350, and (CeO<sub>x</sub>)<sub>0.50</sub>CuO-350 in sequence. For reference, a pure CuO-350 sample was synthesized according to a similar procedure except for the absence of Ce(NO<sub>3</sub>)<sub>3</sub>. The calcination temperature at 350 °C was chosen based on the following considerations: (a) according to our experience, the specific surface area or dispersion of Cu-based composite oxide would be significantly lowered at the calcination temperature beyond 400 °C, and 350 °C was sufficient to obtain phase-stabilized Cu-based composite oxides; (b) current advanced Cu-based catalysts could achieve valuable high conversion for NH<sub>3</sub>-SCR-NO<sub>x</sub> below 350 °C;<sup>19,25</sup> therefore, this temperature was pre-set as a working criterion for estimating the samples prepared in this study. However, according to the estimation of a reviewer on possible high temperature for using, the dried powders of (CeO<sub>x</sub>)<sub>0.25</sub>CuO were also calcined at 400 °C and 450 °C for further investigation, and they were designated as (CeO<sub>x</sub>)<sub>0.25</sub>-CuO-400 and (CeO<sub>x</sub>)<sub>0.25</sub>CuO-450.

### 2.2. Characterization

The actual compositions of the samples were quantified *via* inductively coupled plasma-optical emission spectroscopy (ICP-OES) using an Agilent Technologies 5100 ICP-OES.

X-ray powder diffraction experiments (XRD) were carried out *via* a Persee XD-3 X-ray diffractometer at the scan rate of 1° min<sup>−1</sup> in the angle range of 20–80° using Cu K $\alpha$  radiation.

Chemical states of the sample surface were investigated by X-ray photoelectron spectroscopy (XPS) using an Axis Ultra DLD electron spectrometer. The spectra were obtained at ambient temperature under ultra-high vacuum. During data processing of the XPS spectra, the binding energy was calibrated with reference to the C 1s peak of the contaminant carbon at 284.5 eV.

H<sub>2</sub>-temperature programmed reduction (H<sub>2</sub>-TPR) experiments were performed using a quartz U-type reactor connected to a thermal conductivity detector (TCD) with an Ar–H<sub>2</sub> mixture (10% of H<sub>2</sub> by volume, 30 ml min<sup>−1</sup>) as the reductant. Prior to the reduction, the sample (50 mg) was pre-treated in a high purity N<sub>2</sub> stream at 300 °C for 1 h and then cooled down to room temperature. TPR measurements were carried out from 50 °C to the target temperature at the rate of 10 °C min<sup>−1</sup>.

NH<sub>3</sub>-temperature-programmed-desorption experiments (NH<sub>3</sub>-TPD) were performed *via* a Micromeritics AutoChem II 2920 apparatus. Before analysis, about 50 mg of the sample was pre-treated at 120 °C in a helium stream for 1 h and then cooled



down to room temperature. After absorption of  $\text{NH}_3$  (at room temperature) by a pulsed flow of 0.5%  $\text{NH}_3$  in helium at the flow rate of  $30 \text{ ml min}^{-1}$  for 1 h, the system was purged with helium flow at  $30 \text{ ml min}^{-1}$  for 1 h to remove physically adsorbed  $\text{NH}_3$  and then heated from room temperature to  $800^\circ\text{C}$  at the heating rate of  $10^\circ\text{C min}^{-1}$  to monitor the desorption signals.

### 2.3. Catalytic tests

The catalytic activities of the prepared catalysts for  $\text{NH}_3$ -SCR in excess oxygen were investigated using a fixed-bed quartz reactor and 180 mg of the catalyst (20–30 mesh) was used. The reactant gas was composed of 1000 ppm NO, 1000 ppm  $\text{NH}_3$ , 5 vol%  $\text{O}_2$ , 200 ppm  $\text{SO}_2$  (when used), and balanced  $\text{N}_2$ . The gas hourly space velocity (GHSV) was  $40\,000 \text{ h}^{-1}$ . The concentrations of NO and  $\text{NO}_2$  remaining in the product were analysed by an on-line chemiluminescence-based NO- $\text{NO}_x$  analyzer (Model 42i-HL, Thermo Scientific). For the concentration of the gases at steady state, the NO conversion was calculated as follows:

$$\text{NO conversion} = (1 - [\text{NO}]_{\text{outlet}}/[\text{NO}]_{\text{inlet}}) \times 100\%$$

## 3. Results and discussion

The XRD patterns of  $(\text{CeO}_x)_m\text{CuO}$  (with Ce/Cu molar ratio  $m$  at 0.125, 0.25, and 0.5) and CuO samples are presented in Fig. 1. The diffraction peaks (Fig. 1a) observed at the  $2\theta$  values of  $35.5^\circ$ ,  $38.6^\circ$ ,  $48.8^\circ$ ,  $52.5^\circ$ ,  $58.4^\circ$ , and  $61.6^\circ$  for pure CuO-350 reference sample could be assigned to the crystalline features of monoclinic CuO (JCPDS 45-0937). In contrast, for the  $(\text{CeO}_x)_m\text{CuO}$ -350 samples, with the increasing Ce composition (Fig. 1b–d), obvious and gradual decreases in the intensity for the

diffraction peaks of CuO phase were observed. In addition, there were no notable signals correlated to  $\text{CeO}_x$  diffractions that could be resolved with these samples; however, clear shifts up to  $2\theta$  of  $35.7^\circ$  and  $38.9^\circ$  for two main diffraction peaks compared to those of the pure CuO sample were observed in the  $(\text{CeO}_x)_m\text{CuO}$  samples. Similar observations have also been reported on Cu–Ce/ZSM catalysts, in which the phenomenon was attributed to the effect of Ce doping into the crystalline of copper oxide.<sup>23</sup> Thus, the absence of  $\text{CeO}_x$  diffraction peaks and diffraction shifts compared to the XRD pattern of pure CuO on prepared  $(\text{CeO}_x)_m\text{CuO}$  samples clearly indicated the doping of Ce species into CuO crystalline for these samples, which could be a hint of the presence of interaction between the components of our samples. According to the estimation of a reviewer,  $(\text{CeO}_x)_{0.25}\text{CuO}$ -400 and  $(\text{CeO}_x)_{0.25}\text{CuO}$ -450 (calcined at  $400^\circ\text{C}$  or  $450^\circ\text{C}$ ) were also tested and the results are shown in Fig. 1e and f. Similar diffraction patterns with close peak positions and comparable intensities were found for the three  $(\text{CeO}_x)_{0.25}\text{CuO}$  samples, which manifested phase stability of our samples under the thermal condition of  $350$ – $450^\circ\text{C}$ .

Surface features of the samples were investigated by XPS characterization, as shown in Fig. 2. In contrast to pure CuO, the spectral feature at  $880$ – $920 \text{ eV}$  observed for the  $(\text{CeO}_x)_m\text{CuO}$  samples, as shown in Fig. 2A, corresponds to Ce 3d. These Ce 3d spectra were fitted into ten binding energy (BE) peaks, labelled as v-kind, originated from  $3d_{5/2}$  photoemissions, and the associated  $3d_{3/2}$  emissions are labelled as u-kind. The BE peaks marked as v ( $882.5 \text{ eV}$ ), v' ( $888.9 \text{ eV}$ ), and v'' ( $898.3 \text{ eV}$ ) originated from Ce(IV)  $3d_{5/2}$ , whereas the BE peaks labelled as u ( $901.2 \text{ eV}$ ), u' ( $907.5 \text{ eV}$ ), and u'' ( $916.8 \text{ eV}$ ) originated from Ce(IV)  $3d_{3/2}$ . The v' ( $881.5 \text{ eV}$ )–v'' ( $885.1 \text{ eV}$ ) and u' ( $898.8 \text{ eV}$ )–u'' ( $903.4 \text{ eV}$ ), refer to  $3d_{5/2}$  and  $3d_{3/2}$  of Ce(III), respectively, suggesting the co-presence of Ce(III) and Ce(IV) on  $(\text{CeO}_x)_m\text{CuO}$  samples.<sup>21,26,27</sup> For a CuO reference sample, BEs of  $933.7 \text{ eV}$  and  $953.7 \text{ eV}$  (Fig. 2B) for the two main peaks are close to the standard values of Cu  $2p_{3/2}$  and Cu  $2p_{1/2}$  of CuO, respectively,<sup>28,29</sup> which were accompanied by two shakeup satellite peaks in the range of  $938.2$ – $946.3 \text{ eV}$  and a isolated satellite peak around  $962.1 \text{ eV}$ .  $(\text{CeO}_x)_m\text{CuO}$  samples showed similar peaks, except for the obvious BE shifts of peaks towards lower BE compared to CuO. With careful deconvolution measurements, besides Cu  $2p_{3/2}$  and Cu  $2p_{1/2}$  peaks of CuO, additional peaks located around  $933.4 \text{ eV}$  and  $953.3 \text{ eV}$  were also resolved for the  $(\text{CeO}_x)_m\text{CuO}$  samples. These peaks, with lower BE compared to those of CuO, were close to the BE value of  $\text{Cu}^+$  in the composite oxides reported in the literature,<sup>26,27</sup> suggesting the existence of  $\text{Cu}^+$  on the  $(\text{CeO}_x)_m\text{CuO}$  samples. Among the species on the surface, Ce(III) and  $\text{Cu}^+$  could be more attractive since they are believed to be helpful for creating charge imbalance or promoting active species mobility to facilitate the reaction;<sup>21,29</sup> thus, the contents or distributions of these two species were worthy of further investigation.

Based on the abovementioned peak-fitting measurements, a literature method was applied to estimate the relative concentrations ( $C$ ) of Ce(III) by the calculated peak area of Ce species according to the following equations:<sup>30–33</sup>

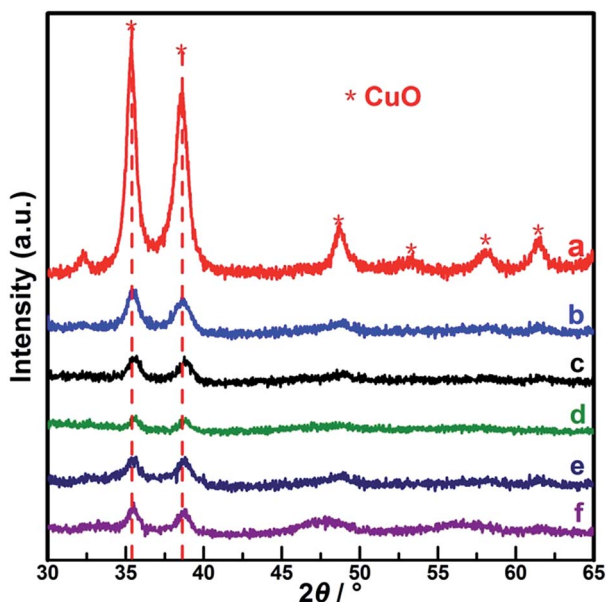


Fig. 1 XRD patterns of samples. (a) CuO, (b)  $(\text{CeO}_x)_{0.125}\text{CuO}$ -350, (c)  $(\text{CeO}_x)_{0.25}\text{CuO}$ -350, (d)  $(\text{CeO}_x)_{0.50}\text{CuO}$ -350, (e)  $(\text{CeO}_x)_{0.25}\text{CuO}$ -400, and (f)  $(\text{CeO}_x)_{0.25}\text{CuO}$ -450.





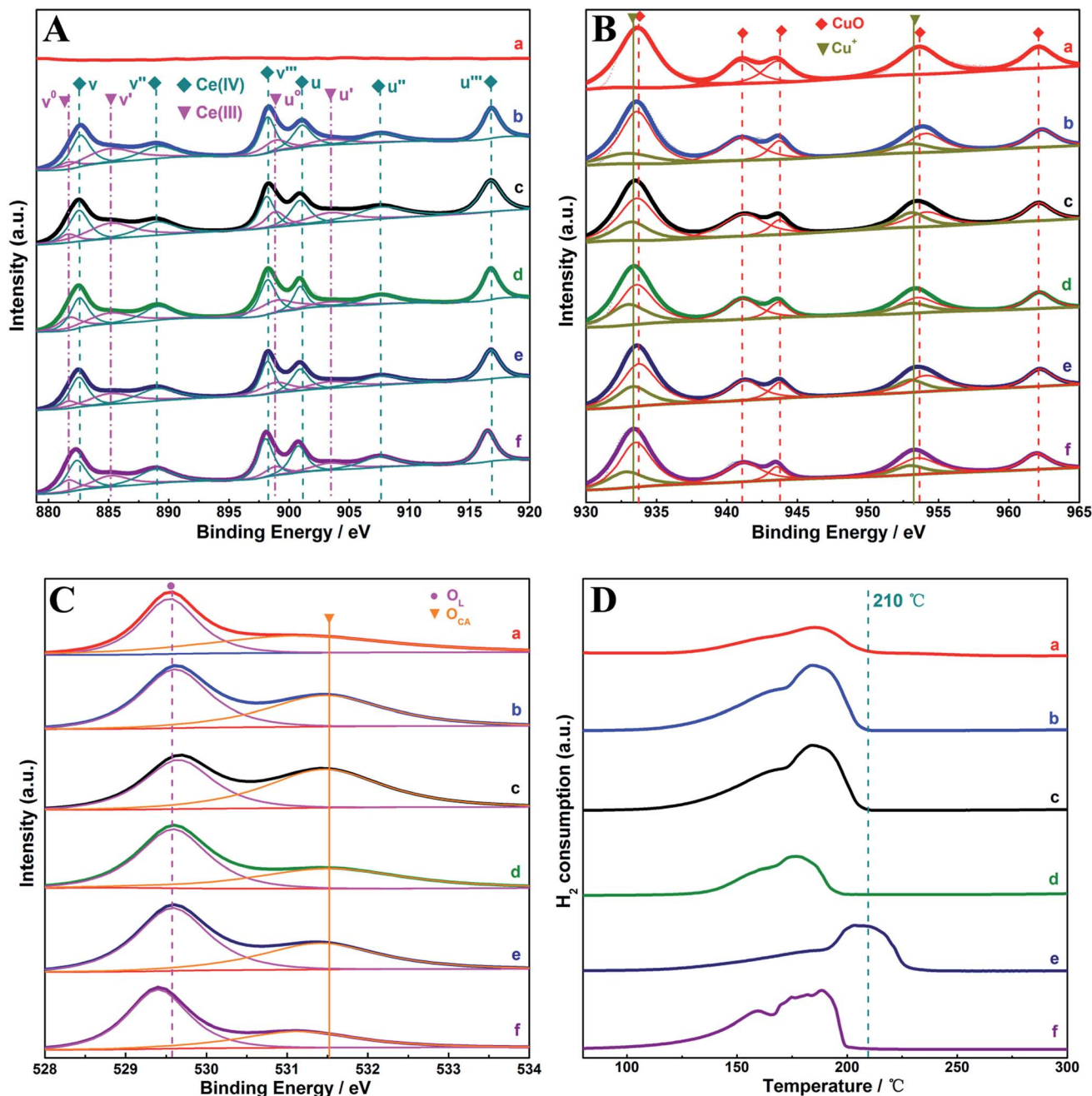


Fig. 2 XPS spectra and H<sub>2</sub>-TPR profiles of the samples. (A) Ce 3d spectra; (B) Cu 2p spectra (C) O 1s spectra. (D) H<sub>2</sub>-TPR profiles (a) CuO, (b) (CeO<sub>x</sub>)<sub>0.125</sub>CuO-350, (c) (CeO<sub>x</sub>)<sub>0.25</sub>CuO-350, (d) (CeO<sub>x</sub>)<sub>0.50</sub>CuO-350, (e) (CeO<sub>x</sub>)<sub>0.25</sub>CuO-400, (f) (CeO<sub>x</sub>)<sub>0.25</sub>CuO-450.

$$A_{\text{Ce(III)}} = A_{\text{v}_0} + A_{\text{u}_0} + A_{\text{v}'} + A_{\text{u}'}$$

$$A_{\text{Ce(IV)}} = A_{\text{v}} + A_{\text{u}} + A_{\text{v}''} + A_{\text{u}''} + A_{\text{v}'''} + A_{\text{u}'''}$$

$$C_{\text{Ce(III)}} = A_{\text{Ce(III)}} / (A_{\text{Ce(IV)}} + A_{\text{Ce(III)}})$$

Similarly, the contents of Cu<sup>+</sup> in the (CeO<sub>x</sub>)<sub>m</sub>-CuO samples were also roughly estimated by the ratio between the sum of the peak area correlated to Cu<sup>+</sup> and total area of the peaks around Cu 2p<sub>3/2</sub> and Cu 2p<sub>1/2</sub>. The corresponding species distributions of samples are listed in Table 1. In general, the increasing Ce

composition among the (CeO<sub>x</sub>)<sub>m</sub>CuO-350 samples ( $m = 0.125, 0.25$ , and  $0.50$ ) resulted in gradually decreased Ce(III) content accompanied by the highest distribution of Cu<sup>+</sup> achieved on (CeO<sub>x</sub>)<sub>0.25</sub>CuO-350, suggesting that controlling the amount of Ce doped into CuO was crucial to confine the presence and distribution of Cu<sup>+</sup> on the surface of the samples. These interactive changes among active components were always accepted as a hint or consequence of the presence of a synergistic effect in the composite samples.<sup>26,27</sup> Note that the synergistic effect in the present samples was distinguished with that of the reported Cu-based NH<sub>3</sub>-SCR-NO<sub>x</sub> catalysts (especially with ternary-

**Table 1** Surface atom concentrations (derived from XPS) and H<sub>2</sub> consumptions (derived from H<sub>2</sub>-TPR) of the samples

Samples	Surface composition (at%)					Con.H <sub>2</sub> <sup>a</sup>	
	Ce (Ce(III)/Ce)	Cu (Cu <sup>+</sup> /Cu)	O (O <sub>CA</sub> /O)				
CuO-350	0	<b>0</b>	39.1	<b>0</b>	60.9	<b>34.1</b>	1
(CeO <sub>x</sub> ) <sub>0.125</sub> CuO-350	8.5	<b>41.5</b>	24.7	<b>18.8</b>	66.8	<b>49.4</b>	2.2
(CeO <sub>x</sub> ) <sub>0.25</sub> CuO-350	9.8	<b>40.1</b>	21.2	<b>27.2</b>	69.0	<b>57.8</b>	2.6
(CeO <sub>x</sub> ) <sub>0.50</sub> CuO-350	15.0	<b>27.7</b>	18.9	<b>23.4</b>	66.1	<b>41.7</b>	1.4
(CeO <sub>x</sub> ) <sub>0.25</sub> CuO-400	13.1	<b>30.8</b>	22.3	<b>22.5</b>	64.6	<b>42.9</b>	1.5
(CeO <sub>x</sub> ) <sub>0.25</sub> CuO-450	12.4	<b>30.5</b>	24.8	<b>19.3</b>	62.8	<b>35.3</b>	1.7

<sup>a</sup> The relative consumptions of H<sub>2</sub> (Con.H<sub>2</sub>) on the samples were calibrated by the ratio between Con.H<sub>2</sub> peak area of the samples and that of the reference CuO-350 sample.

component samples) since one of the main features of the synergistic effect in these catalysts was embodied by the presence of isolated Cu<sup>2+</sup> (with higher BE compared to that of CuO).<sup>27,29</sup> In addition, the synergistic effect in composite structures would also influence the distribution of other active species in the samples such as active oxygen species required for redox reactions. The oxygen spectra of the prepared samples are shown in Fig. 2C, where lattice oxygen O<sub>L</sub> (528.0–531.5 eV) and chemisorbed oxygen O<sub>CA</sub> (529.0–533.7 eV) were fitted for all the samples,<sup>34–36</sup> and the corresponding distributions are listed in Table 1. It is clear that higher concentrations of chemisorbed oxygen were distributed on (CeO<sub>x</sub>)<sub>m</sub>CuO-350 samples compared to those on CuO-350, and (CeO<sub>x</sub>)<sub>0.25</sub>CuO-350 showed the highest concentration of chemisorbed oxygen. Considering that chemisorbed oxygen was one of the key active species for most redox reactions, the result further manifested that doping Ce into CuO in a proper way to modulate the distribution of Cu<sup>+</sup> on the surface of the present samples could be beneficial to optimize their surface state for the reactions. For (CeO<sub>x</sub>)<sub>0.25</sub>CuO samples obtained employing different temperature, with the increase of processing temperature, both the contents of Ce(III) and Cu<sup>+</sup> were lowered, and the trend was accompanied by a decrease in the concentration of O<sub>CA</sub>, suggesting that the higher calcination temperature would negatively influence the surface distribution of the active species in the present Cu–Ce composite oxides.

The influence of the surface distribution of active species on the redox properties of the samples was investigated by H<sub>2</sub>-TPR, and the results are shown in Fig. 2D. The main H<sub>2</sub> consumption peaks are located in temperature range of 100–210 °C for all the samples except for (CeO<sub>x</sub>)<sub>0.25</sub>CuO-400 (extended to 230 °C), which was quite low compared to the temperature of reduced bulk CuO or Ce species reported on Cu-based composites.<sup>21,27,37–39</sup> Thus, these features could be excluded for our samples. Generally, the H<sub>2</sub> consumption peaks below 260 °C for the reported Cu–Ce composite samples are attributed to the reduction of well-dispersed surface Cu species or active Cu species, such as Cu<sup>2+</sup>, on Cu–Ce interface.<sup>21,27,38</sup> Obviously, these species were difficult to be estimated for the current samples according to previous XPS measurements. To illuminate the

origin of H<sub>2</sub>-TPR features for our samples, the relative consumptions of H<sub>2</sub> (Con.H<sub>2</sub>) for the samples were calibrated by the ratio between Con.H<sub>2</sub> peak area of samples and that of reference CuO-350 sample, and the results are listed in Table 1. From the data shown in the Table, even assuming that O<sub>CA</sub> was very sensitive to consume H<sub>2</sub>, the change of amounts of O<sub>CA</sub> among the samples was not sufficient to solely afford the corresponding alternations in the H<sub>2</sub>-consumption. Interestingly, the Con.H<sub>2</sub> values among the samples were roughly governed by the sum of the contents of Cu<sup>+</sup> and O<sub>CA</sub>, *i.e.*, the higher the sum of the contents, the higher the H<sub>2</sub>-consumption; this dependence directly indicated that Cu<sup>+</sup> was one of the significant species to react with H<sub>2</sub> on the present samples. The point could be demonstrated by the comparison between the (CeO<sub>x</sub>)<sub>0.25</sub>CuO-450 and reference CuO-350 samples. Although higher calcination temperature caused some deviation for (CeO<sub>x</sub>)<sub>0.25</sub>CuO-450 in contrast to the abovementioned dependence, with the baseline that O<sub>CA</sub> content on (CeO<sub>x</sub>)<sub>0.25</sub>CuO-450 and CuO-350 were close to each other, the much higher H<sub>2</sub>-consumption for (CeO<sub>x</sub>)<sub>0.25</sub>CuO-450 is directly linked to the additional Cu<sup>+</sup> content on the sample compared to that on CuO-350. Therefore, it was reasonable to propose that the redox properties of the present Cu–Ce composite oxide were directly connected with the existence and distribution of Cu<sup>+</sup> on the surface of the present samples.

Considering that the surface acid property of the catalyst was crucial for NH<sub>3</sub>-SCR-NO<sub>x</sub>, NH<sub>3</sub>-TPD tests were performed for our samples, and the results are shown in Fig. 3. For CuO-350, the broad and weak desorption peak observed at 150–350 °C could be attributed to the feature of weak Brønsted acid sites on the CuO surface; in contrast, the desorption peaks of NH<sub>3</sub> in 350–450 °C were exhibited for the three (CeO<sub>x</sub>)<sub>m</sub>CuO-350 samples,

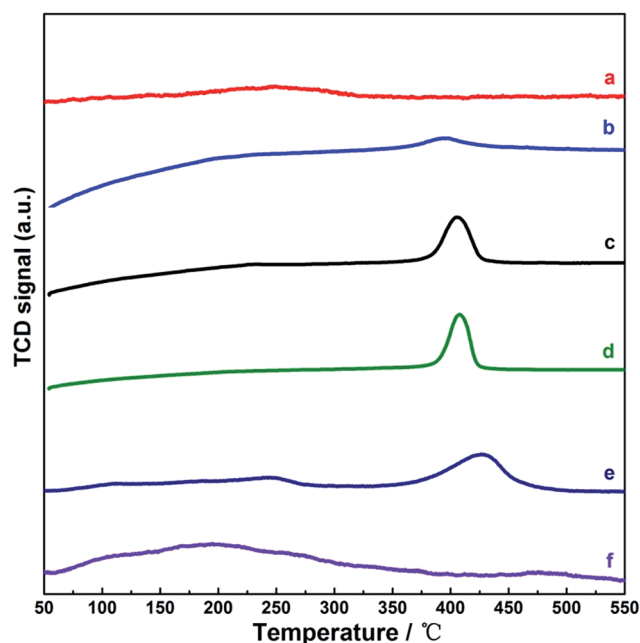


**Fig. 3** NH<sub>3</sub>-TPD profiles for the samples. (a) CuO, (b) (CeO<sub>x</sub>)<sub>0.125</sub>CuO-350, (c) (CeO<sub>x</sub>)<sub>0.25</sub>CuO-350, (d) (CeO<sub>x</sub>)<sub>0.50</sub>CuO-350, (e) (CeO<sub>x</sub>)<sub>0.25</sub>CuO-400, and (f) (CeO<sub>x</sub>)<sub>0.25</sub>CuO-450.



which were related to the structural Brønsted acid sites inferred to moderate and strong acidity or Lewis acid sites.<sup>25,40–42</sup> According to the peak areas for  $\text{NH}_3$  desorption, a five-fold change in the desorption (or adsorption) amount of  $\text{NH}_3$  emerged by increasing the Ce composition with  $m$  ranging from 0.125 to 0.25 for the  $(\text{CeO}_x)_m\text{CuO}$ -350 samples was observed; however, only a 1.2-fold increase in the desorption amount of  $\text{NH}_3$  was observed on increasing  $m$  from 0.25 to 0.50. These results suggested that a 0.25 Ce/Cu molar ratio was the key composition to obtain the desired distribution of the acid sites in the present samples. Note that the sums of surface concentration of  $\text{Ce(III)}$  and  $\text{Cu}^+$  on  $(\text{CeO}_x)_{0.25}\text{CuO}$ -350 and  $(\text{CeO}_x)_{0.50}\text{CuO}$ -350 were close to each other, but were higher than those of  $(\text{CeO}_x)_{0.125}\text{CuO}$ -350 (Table 1). In view of the  $\text{Ce(III)}$  species or isolated transition metal ions in the composite oxides generally accepted as the resource to produce acid surface (Lewis acid sites),<sup>26,29</sup> the observed differences of the acid amount in these  $(\text{CeO}_x)_m\text{CuO}$ -350 samples could be attributed to the different distribution of the acid source species such as  $\text{Ce(III)}$  species and  $\text{Cu}^+$  on the samples. Moreover, for the  $(\text{CeO}_x)_{0.25}\text{CuO}$  samples prepared at different calcination temperatures (Fig. 3c, e and f), the sum of the  $\text{Ce(III)}$  species and  $\text{Cu}^+$  concentration in the samples decreased with the increasing calcination temperature, which was accompanied by the lowered acid amount (desorption amount of  $\text{NH}_3$ ) and weakened acidity ( $\text{NH}_3$  desorption at low temperature). This connection further confirmed the proportional dependence of the sum distribution of  $\text{Ce(III)}$  species and  $\text{Cu}^+$  on the surface acid properties among our samples. These results also suggested that the surfaces of the  $(\text{CeO}_x)_m\text{CuO}$ -350 and  $(\text{CeO}_x)_{0.25}\text{CuO}$ -400 samples were dominated by Lewis acid sites.

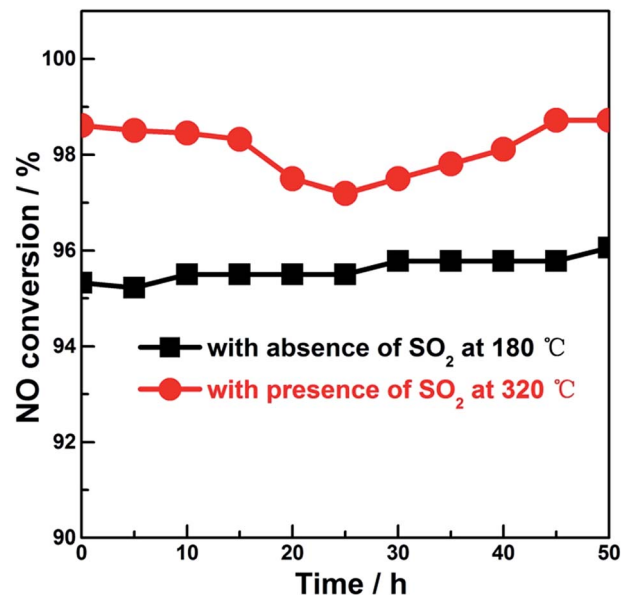


Fig. 5 NO conversion as a function of time over  $(\text{CeO}_x)_{0.25}\text{CuO}$ -350.

The catalytic performances of the samples were investigated for  $\text{NH}_3$ -SCR-NO in the absence and presence of  $\text{SO}_2$ , which is shown in Fig. 4A and B. For reaction in the absence of  $\text{SO}_2$  (Fig. 4A), in contrast to the low NO conversion (not more than 70%) over  $\text{CuO}$ -350, all the Ce-introduced samples could achieve NO conversion beyond 80% within the temperature window of 130–230 °C. Among the  $(\text{CeO}_x)_m\text{CuO}$ -350 samples, the best performance (the highest NO conversion and the broadest temperature window) was observed for  $(\text{CeO}_x)_{0.25}\text{CuO}$ -

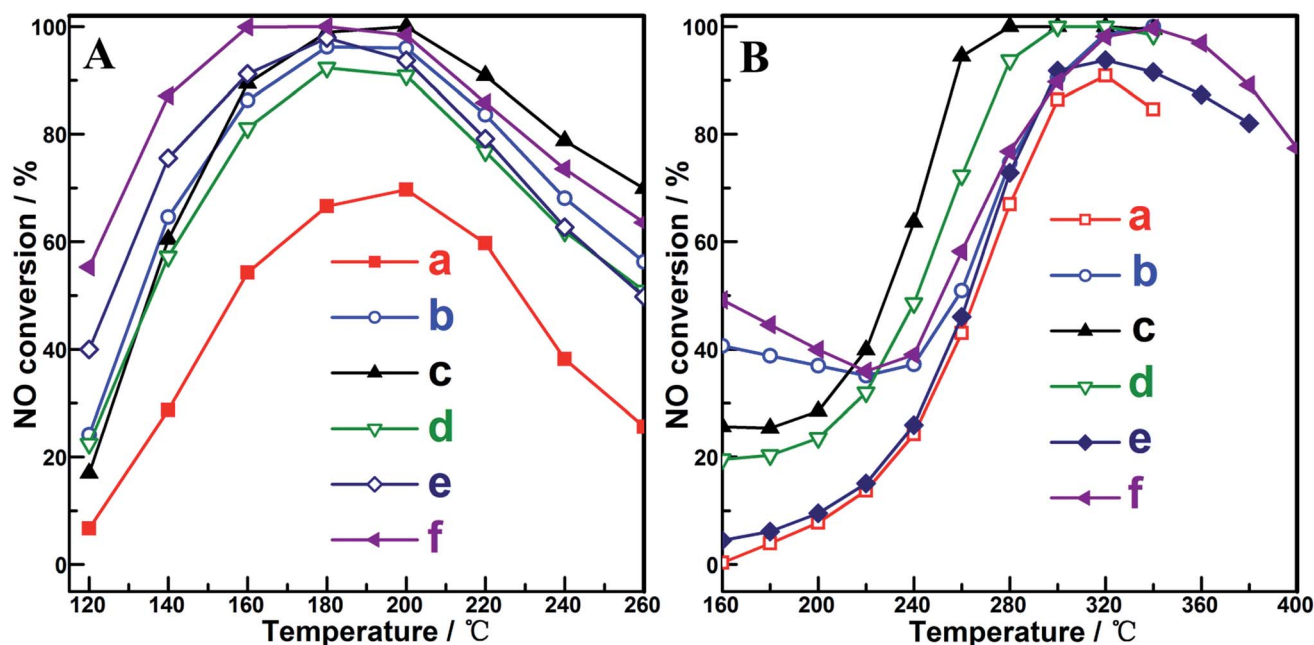


Fig. 4 Dependence of NO conversion on reaction temperature with (A)  $\text{SO}_2$ -absence and (B)  $\text{SO}_2$ -presence. Reaction conditions:  $[\text{NO}] = [\text{NH}_3] = 1000$  ppm,  $[\text{O}_2] = 5\%$ ,  $[\text{SO}_2] = 200$  ppm (when used), GHSV = 40 000  $\text{h}^{-1}$ . (a)  $\text{CuO}$ , (b)  $(\text{CeO}_x)_{0.125}\text{CuO}$ -350, (c)  $(\text{CeO}_x)_{0.25}\text{CuO}$ -350, (d)  $(\text{CeO}_x)_{0.50}\text{CuO}$ -350, (e)  $(\text{CeO}_x)_{0.25}\text{CuO}$ -400, and (f)  $(\text{CeO}_x)_{0.25}\text{CuO}$ -450.





**Table 2** Preparation details of various Cu-based NH<sub>3</sub>-SCR-NO catalysts and corresponding catalytic measurements in the presence of SO<sub>2</sub>

Catalysts	Preparation method	Features of samples	Reaction condition	Temperature window <sup>a</sup>	Final conversion of NO <sup>b</sup>	References
Ce-Fe/WMH	Two-step impregnation	Enrichment of Ce <sup>3+</sup> on catalyst surface	1000 ppm NO, 1000 ppm NH <sub>3</sub> , 100, 500, and 1000 ppm (when used) SO <sub>2</sub> and 3 vol% O <sub>2</sub> balanced with N <sub>2</sub> , GHSV at 10 000 h <sup>-1</sup>	250 °C	92%	46
Ni-Ce-La composite oxide	Mulsifier-free emulsion polymerization	More lattice defects	1000 ppm NO, 1000 ppm NH <sub>3</sub> , 500 ppm SO <sub>2</sub> and 5 vol% O <sub>2</sub> balanced with N <sub>2</sub> , GHSV at 20 000 h <sup>-1</sup>	300 °C	90%	47
SnO <sub>2</sub> -MnO <sub>x</sub> -CeO <sub>2</sub>	Co-precipitation	Crystallinity loss	1000 ppm NO, 1000 ppm NH <sub>3</sub> , 100 ppm SO <sub>2</sub> , 2 vol% O <sub>2</sub> balanced with N <sub>2</sub> , GHSV at 35 000 h <sup>-1</sup>	220 °C	94%	48
MeO <sub>x</sub> -MnO <sub>x</sub> /SAPO-34 (Me = Pr or Ce)	Solvent dispersion	Rich in oxygen vacancies	800 ppm NO, 800 ppm NH <sub>3</sub> , 100 ppm SO <sub>2</sub> and 5 vol% O <sub>2</sub> balanced with Ar, GHSV at 40 000 h <sup>-1</sup>	200 °C	60.5%	49
Ce-Cu composite oxides	Co-precipitation	Cu <sup>+</sup> on the surface of Ce-doped CuO	1000 ppm NO, 1000 ppm NH <sub>3</sub> , 200 ppm SO <sub>2</sub> and 5 vol% O <sub>2</sub> balanced with N <sub>2</sub> , GHSV at 40 000 h <sup>-1</sup>	250–350 °C	98%	This work

<sup>a</sup> The temperature range for NO conversion beyond 80%. <sup>b</sup> The highest NO conversion.

350, which could be attributed to the outstanding distribution of the active species such as Ce(III), Cu<sup>+</sup>, and O<sub>CA</sub>, and the corresponding optimized redox and surface acid properties of the sample. For the (CeO<sub>x</sub>)<sub>0.25</sub>CuO samples obtained at 400 °C and 450 °C, the higher NO conversion on these compared to that on (CeO<sub>x</sub>)<sub>0.25</sub>CuO-350 could be correlated to the more obvious feature of the weak acid sites observed in the low temperature range of 80–300 °C on these samples (seen in the NH<sub>3</sub>-TPD profiles of Fig. 3e and f) since it was found that weak acid sites on the samples were sufficient to accomplish NH<sub>3</sub>-SCR-NO at low reaction temperature.<sup>19,43</sup> Considering that SO<sub>2</sub> was always present in normal NH<sub>3</sub>-SCR-NO<sub>x</sub> processes and a main challenge for current Cu-based catalysts is their poor SO<sub>2</sub> resistance, more practical and meaningful performance of NH<sub>3</sub>-SCR-NO<sub>x</sub> Cu-based catalysts should be focused on the catalytic behaviour in the presence of SO<sub>2</sub>. As shown in Fig. 4B, meaningful conversion of NO (beyond 80%) in the presence of SO<sub>2</sub> on the samples was all shifted to the high temperature range (beyond 240 °C) compared to that in the absence of SO<sub>2</sub>, and the best SO<sub>2</sub>-resistant NH<sub>3</sub>-SCR-NO performance with NO conversion close to 100% in the temperature window of 250–350 °C was obtained on (CeO<sub>x</sub>)<sub>0.25</sub>CuO-350 among the samples. The surface acid feature of catalyst was found to be the decisive factor that governed the performance of NH<sub>3</sub>-SCR-NO<sub>x</sub>. In our study, the acid amount on (CeO<sub>x</sub>)<sub>0.50</sub>CuO-350 was higher than that on (CeO<sub>x</sub>)<sub>0.25</sub>CuO-350; however, the SO<sub>2</sub> resistance and NO converting performance between two samples followed an opposite order, suggesting that the acid feature was not the only significant factor affecting the SO<sub>2</sub>-resistant NH<sub>3</sub>-SCR-NO. In contrast, the order of SO<sub>2</sub>-resistant performance among our samples approximately followed their Cu<sup>+</sup> concentration sequence. The outstanding SO<sub>2</sub>-resistant performance of (CeO<sub>x</sub>)<sub>0.25</sub>CuO-350 could be correlated to its highest surface distribution of Cu<sup>+</sup> among the samples. The correlation is in agreement with the recent findings on SO<sub>2</sub>-removal on Cu-containing composites, in which the existence of

Cu<sup>+</sup> in a notable amount was demonstrated to be crucial for the chemical removal of SO<sub>2</sub> due to its positive role in transferring charge or active oxygen species through the Cu(I)–Cu(II) redox cycle.<sup>44,45</sup> The steady-state performance of (CeO<sub>x</sub>)<sub>0.25</sub>CuO-350 was further investigated under SO<sub>2</sub>-absence and SO<sub>2</sub>-presence conditions, as shown in Fig. 5. For both cases, the slight fluctuations within 2% were obtained on the sample, exhibiting the desired application stability of the present samples. In view of estimating the influence of the gas hourly space velocity (GHSV) on SO<sub>2</sub>-resistant NH<sub>3</sub>-SCR-NO performance from a reviewer, some typical studies were surveyed and are listed in Table 2. Although the GHSV employed in this study was in the middle rank compared with literature works, the higher concentration of SO<sub>2</sub> in the reactant gas could ensure the kinetic estimation for the present samples. The comparable high NO conversion in the presence of higher concentration of SO<sub>2</sub> obtained in the present (CeO<sub>x</sub>)<sub>m</sub>CuO samples suggested that these samples are a type of efficient and notable SO<sub>2</sub>-resistant NH<sub>3</sub>-SCR-NO<sub>x</sub> catalyst, especially in view of the distinguished Cu<sup>+</sup> distributions on the samples.

## 4. Conclusions

The synergistic effect involved in the present Cu–Ce composite structures, prepared *via* a common co-precipitation method, were found to be pronounced for producing distinguished Cu<sup>+</sup> species on the surface of Ce-doped CuO. The distribution of Cu<sup>+</sup> could be modulated by controlling the amount of Ce introduced, which was functional to optimize the redox and surface acid features of the samples, leading to outstanding SO<sub>2</sub>-resistant NH<sub>3</sub>-SCR-NO performance. These findings could serve for understanding the catalytic behaviour of Cu–Ce composite catalysts as well as innovating more efficient Cu-based catalysts for NH<sub>3</sub>-SCR-NO<sub>x</sub> and other heterogeneous catalysis applications upon Cu catalysts.



## Acknowledgements

Authors gratefully acknowledge the financial support of the National Natural Science Foundation of China (NSFC, No. 21003071 and No. 21563018) and Doctoral Fund of the Ministry of Education of China (No. 20093601120007).

## Notes and references

- 1 P. Forzatti, I. Nova and E. Tronconi, *Angew. Chem., Int. Ed.*, 2009, **48**, 8366–8368.
- 2 B. Li, Z. Ren, Z. Ma, X. Huang, F. Liu, X. Zhang and H. Yang, *Catal. Sci. Technol.*, 2016, **6**, 1719–1725.
- 3 G. S. Qi, R. T. Yang and R. Chang, *Appl. Catal., B*, 2004, **51**, 93–106.
- 4 M. H. Kim and T. H. An, *Res. Chem. Intermed.*, 2011, **37**, 1333–1344.
- 5 M. Q. Shen, C. X. Li, J. Q. Wang, L. L. Xu, W. L. Wang and J. Wang, *RSC Adv.*, 2015, **5**, 35155–35165.
- 6 L. Chen, J. Li and M. Ge, *J. Phys. Chem. C*, 2009, **113**, 21177–21184.
- 7 B. J. Dou, G. Lv, C. Wang, Q. L. Hao and K. S. Hui, *Chem. Eng. J.*, 2015, **270**, 549–556.
- 8 T. Yu, M. Xu, Y. Huang, J. Wang, J. Wang, L. Lv, G. Qi, W. Li and M. Shen, *Appl. Catal., B*, 2017, **204**, 525–536.
- 9 Q. Zhang, L. Xu, P. Ning, J. Gu and Q. Guan, *Appl. Surf. Sci.*, 2014, **317**, 955–961.
- 10 T. Guenter, J. Pesek, K. Schaefer, A. B. Abai, M. Casapu, O. Deutschmann and J.-D. Grunwaldt, *Appl. Catal., B*, 2016, **198**, 548–557.
- 11 L. Xu, C. Shi, B. Chen, Q. Zhao, Y. Zhu, H. Gies, F.-S. Xiao, D. De Vos, T. Yokoi, X. Bao, U. Kolb, M. Feyen, S. Maurer, A. Moini, U. Müller and W. Zhang, *Microporous Mesoporous Mater.*, 2016, **236**, 211–217.
- 12 B. Thirupathi and P. G. Smirniotis, *Appl. Catal., B*, 2011, **110**, 195–206.
- 13 Y. Zhu, Y. Zhang, R. Xiao, T. Huang and K. Shen, *Catal. Commun.*, 2017, **88**, 64–67.
- 14 L. Qiu, J. Meng, D. Pang, C. Zhang and F. Ouyang, *Catal. Lett.*, 2015, **145**, 1500–1509.
- 15 L. Pang, C. Fan, L. Shao, K. Song, J. Yi, X. Cai, J. Wang, M. Kang and T. Li, *Chem. Eng. J.*, 2014, **253**, 394–401.
- 16 L. Huang, X. Wang, S. Yao, B. Jiang, X. Chen and X. Wang, *Catal. Commun.*, 2016, **81**, 54–57.
- 17 X. Feng, Y. Cao, L. Lan, C. Lin, Y. Li, H. Xu, M. Gong and Y. Chen, *Chem. Eng. J.*, 2016, **302**, 697–706.
- 18 P. Sudarsanam, B. Hillary, B. Mallesham, B. G. Rao, M. H. Amin, A. Nafady, A. M. Alsalmeh, B. M. Reddy and S. K. Bhargava, *Langmuir*, 2016, **32**, 2208–2215.
- 19 W.-g. Pan, Y. Zhou, R.-t. Guo, W.-l. Zhen, J.-n. Hong, H.-j. Xu, Q. Jin, C.-g. Ding and S.-y. Guo, *Environ. Prog. Sustainable Energy*, 2014, **33**, 385–389.
- 20 J. Liu, X. Li, Q. Zhao, D. Zhang and P. Ndokoye, *J. Mol. Catal. A: Chem.*, 2013, **378**, 115–123.
- 21 H. Li, S. Wu, L. Li, J. Wang, W. Ma and K. Shih, *Catal. Sci. Technol.*, 2015, **5**, 5129–5138.
- 22 A. Sultana, M. Sasaki, K. Suzuki and H. Hamada, *Catal. Commun.*, 2013, **41**, 21–25.
- 23 S. Lai, D. Meng, W. Zhan, Y. Guo, Y. Guo, Z. Zhang and G. Lu, *RSC Adv.*, 2015, **5**, 90235–90244.
- 24 X. Gao, X.-s. Du, L.-w. Cui, Y.-c. Fu, Z.-y. Luo and K.-f. Cen, *Catal. Commun.*, 2010, **12**, 255–258.
- 25 R.-t. Guo, W.-l. Zhen, W.-g. Pan, Y. Zhou, J.-n. Hong, H.-j. Xu, Q. Jin, C.-g. Ding and S.-y. Guo, *J. Ind. Eng. Chem.*, 2014, **20**, 1577–1580.
- 26 F. Wang, R. Buchel, A. Savitsky, M. Zalibera, D. Widmann, S. E. Pratsinis, W. Lubitz and F. Schueth, *ACS Catal.*, 2016, **6**, 3520–3530.
- 27 X. Ma, X. Feng, X. He, H. Guo, L. Lv, J. Guo, H. Cao and T. Zhou, *Microporous Mesoporous Mater.*, 2012, **158**, 214–218.
- 28 W. Yao, Y. Zhang, T. Duan, W. Zhu, Z. Yi and X. Cui, *Phys. B*, 2016, **493**, 7–13.
- 29 D. Zhou, B. Li, Z. Ma, X. Huang, X. Zhang and H. Yang, *J. Mol. Catal. A: Chem.*, 2015, **409**, 183–190.
- 30 L. Zhang, T. Chen, S. Zeng and H. Su, *J. Environ. Chem. Eng.*, 2016, **4**, 2785–2794.
- 31 F. Pagliuca, P. Luches and S. Valeri, *Surf. Sci.*, 2013, **607**, 164–169.
- 32 V. A. V. Chauvaut, H. Schneider, M. Cassir, H. Ardeâ Leâ An and A. Galtayries, *J. Appl. Electrochem.*, 2000, **30**, 1405–1413.
- 33 C. Anandan and P. Bera, *Appl. Surf. Sci.*, 2013, **283**, 297–303.
- 34 S. H. O. D. R. Mullins and D. R. Huntley, *Surf. Sci.*, 1998, **409**, 307–319.
- 35 A. Kumar, S. Babu, A. S. Karakoti, A. Schulte and S. Seal, *Langmuir*, 2009, **25**, 10998–11007.
- 36 F. Zhang, G. Tian, H. Wang, H. Wang, C. Zhang, Y. Cui, J. Huang and Y. Shu, *Chem. Res. Chin. Univ.*, 2016, **32**, 461–467.
- 37 J. Wang, L. Cheng, W. An, J. Xu and Y. Men, *Catal. Sci. Technol.*, 2016, **6**, 7342–7350.
- 38 S. H. Zeng, W. L. Zhang, M. Sliwa and H. Q. Su, *Int. J. Hydrogen Energy*, 2013, **38**, 3597–3605.
- 39 C. G. Maciel, T. d. F. Silva, L. P. Roberto Profeti, E. M. Assaf and J. M. Assaf, *Appl. Catal., A*, 2012, **431**, 25–32.
- 40 X.-s. Du, X. Gao, L.-w. Cui, Y.-c. Fu, Z.-y. Luo and K.-f. Cen, *Fuel*, 2012, **92**, 49–55.
- 41 T. Yu, J. Wang, M. Shen and W. Li, *Catal. Sci. Technol.*, 2013, **3**, 3234.
- 42 M. Mhamdi, S. Khaddar-Zine and A. Ghorbel, *Appl. Catal., A*, 2009, **357**, 42–50.
- 43 L. Chen, Z. Si, X. Wu and D. Weng, *ACS Appl. Mater. Interfaces*, 2014, **6**, 8134–8145.
- 44 P. Gaudin, S. Dorge, H. Nouali, D. Kehrli, L. Michelin, L. Josien, P. Fioux, L. Vidal, M. Soulard, M. Vierling, M. Molière, J.-F. Brillhac and J. Patarin, *Appl. Catal., A*, 2015, **504**, 110–118.
- 45 A. Kumar, M. A. Smith, K. Kamasamudram, N. W. Currier and A. Yezerets, *Catal. Today*, 2016, **267**, 10–16.
- 46 Y. Shu, T. Aikebaier, X. Quan, S. Chen and H. Yu, *Appl. Catal., B*, 2014, **150**, 630–635.
- 47 L. Zhang, H. Qu, T. Du, W. Ma and Q. Zhong, *Chem. Eng. J.*, 2016, **296**, 122–131.
- 48 H. Chang, J. Li, X. Chen, L. Ma, S. Yang, J. W. Schwank and J. Hao, *Catal. Commun.*, 2012, **27**, 54–57.
- 49 C. Yu, B. Huang, L. Dong, F. Chen, Y. Yang, Y. Fan, Y. Yang, X. Liu and X. Wang, *Chem. Eng. J.*, 2017, **316**, 1059–1068.

